Reducing posttreatment relapse in cleft lip palatal expansion using an injectable estrogen–nanodiamond hydrogel

Christine Hong[a,1,2], Dayoung Song[a,1], Dong-Keun Lee[b], Lawrence Lin[a], Hsin Chuan Pan[a], Deborah Lee[a], Peng Deng[c], Zhenqing Liu[c], Danny Hadaya[d], Hye-Lim Lee[e], Abdulaziz Mohammad[a], Xinli Zhang[a], Min Lee[b], Cun-Yu Wang[c], and Dean Ho[b,c,f,g,h]

[a]Section of Orthodontics, Division of Growth and Development, School of Dentistry, University of California, Los Angeles, CA 90095; [b]Division of Advanced Prosthodontics, School of Dentistry, University of California, Los Angeles, CA 90095; [c]Division of Oral Biology and Medicine, School of Dentistry, University of California, Los Angeles, CA 90095; [d]Division of Diagnostic and Surgical Sciences, School of Dentistry, University of California, Los Angeles, CA 90095; [e]Sue and Bill Gross Stem Cell Research Center, University of California, Irvine, CA 92697; [f]Department of Bioengineering, Henry Samueli School of Engineering and Applied Science, University of California, Los Angeles, CA 90095; [g]Jonsson Comprehensive Cancer Center, University of California, Los Angeles, CA 90095; and [h]California NanoSystems Institute, University of California, Los Angeles, CA 90095

Edited by George C. Schatz, Northwestern University, Evanston, IL, and approved July 21, 2017 (received for review March 21, 2017)

Patients with cleft lip and/or palate (CLP), who undergo numerous medical interventions from infancy, can suffer from lifelong debilitation caused by underdeveloped maxillae. Conventional treatment approaches use maxillary expansion techniques to develop normal speech, achieve functional occlusion for nutrition intake, and improve esthetics. However, as patients with CLP congenitally lack bone in the cleft site with diminished capacity for bone formation in the expanded palate, more than 80% of the patient population experiences significant postexpansion relapse. While such relapse has been a long-standing battle in craniofacial care of patients, currently there are no available strategies to address this pervasive problem. Estrogen, 17β-estradiol (E2), is a powerful therapeutic agent that plays a critical role in bone homeostasis. However, E2's clinical application is less appreciated due to several limitations, including its pleiotropic effects and short half-life. Here, we developed a treatment strategy using an injectable system with photo–cross-linkable hydrogel (G) and nanodiamond (ND) technology to facilitate the targeted and sustained delivery of E2 to promote bone formation. In a preclinical expansion/relapse model, this functionalized E2/ND/G complex substantially reduced postexpansion relapse by nearly threefold through enhancements in sutural remodeling compared with unmodified E2 administration. The E2/ND/G group demonstrated greater bone volume by twofold and higher osteoblast number by threefold, compared with the control group. The E2/ND/G platform maximized the beneficial effects of E2 through its extended release with superior efficacy and safety at the local level. This broadly applicable E2 delivery platform shows promise as an adjuvant therapy in craniofacial care of patients.

nanomedicine | cleft palate | craniofacial medicine | nanodiamond | drug delivery

With an incidence of 1 in 700 births, cleft lip and/or palate (CLP), caused by failure of fusion between maxillary and nasal processes, is the most common congenital anomaly involving the craniofacial region (1, 2). Affected patients can suffer from a multitude of lifelong challenges due to the constrained growth of the upper jaw (3–5). Thus, maxillary expansion in patients with cleft palate is essential as it contributes to improved speech development, nasal breathing, masticatory function, facilitation of future permanent tooth eruption, and enhanced esthetics leading to greater self-esteem (6). However, the expanded palate has a strong tendency to rebound to its original shape, leading to relapse (7–10). Such compromised stability of expansion remains a significant clinical challenge as it is reported that only 20% of the CLP population retains palatal expansion (7, 11, 12). In addition, studies have reported continued decline in maxillary width up to 5 y following expansion (8). Consequently, relapse frequently necessitates additional expansion and surgical procedures accompanied by critical complications and morbidities.

Patients with CLP are especially susceptible to expansion instability and insufficient bone formation due to congenitally missing bone in the cleft site (11, 12). Therefore, some clinical studies have recommended compensatory overexpansion or longer retention periods of up to 24–36 mo in patients with CLP (12). However, such protocols can result in treatment fatigue and complications, proving to be unfavorable for patients. As the rate and quality of bone formation during and after maxillary expansion significantly impacts posttreatment relapse (12), the use of pro-osteogenic materials in conjunction with conventional expansion mechanics has been actively explored. In particular, estrogen, a naturally occurring steroid, holds great promise due to its well-known benefits in bone homeostasis (13, 14). However, estrogen is a pleiotropic hormone that has multiple physiological functions (15) and its effects in the body are dependent on its route of administration (16). When taken orally, most 17β-estradiol (E2) is converted in the liver into estrone (E1), which is 10-fold less potent than E2 (17). In addition, the resulting supraphysiological level of estrogen in the

Significance

Patients with cleft lip and/or palate require palatal expansion to develop normal speech and fully functional occlusion. However, the expanded palate has a strong tendency to rebound to its original shape due to the patient's congenital lack of bone and diminished capability of bone regeneration in the cleft site. We propose an innovative method to combat this clinical challenge by utilizing estrogen, 17β-estradiol (E2), which has proven bone-building properties, within a nanodiamond–hydrogel (ND/G) complex vehicle. Our study shows that this targeted administration of E2 is able to markedly reduce postexpansion relapse. The demonstrated biocompatibility and efficacy of the E2/ND/G platform makes this a clinically promising solution in craniofacial care of patients.

Author contributions: C.H., X.Z., M.L., and D. Ho designed research; C.H., D.S., D.-K.L., L.L., P.D., Z.L., H.-L.L., and A.M. performed research; C.H., H.C.P., M.L., C.-Y.W., and D. Ho contributed new reagents/analytic tools; C.H., D.S., D.-K.L., L.L., H.C.P., D.L., P.D., Z.L., D. Hadaya, X.Z., M.L., and D. Ho analyzed data; and C.H., D.S., D.-K.L., L.L., D.L., X.Z., and D. Ho wrote the paper.

Conflict of interest statement: D. Ho is a coinventor of issued and pending patents pertaining to nanodiamond drug delivery and imaging.

This article is a PNAS Direct Submission.

Freely available online through the PNAS open access option.

[1]C.H. and D.S. contributed equally to this work.

[2]To whom correspondence should be addressed. Email: chong@dentistry.ucla.edu.

This article contains supporting information online at www.pnas.org/lookup/suppl/doi:10.1073/pnas.1704027114/-/DCSupplemental.

liver increases the risk of blood clots (18, 19) and suppresses growth hormone-mediated insulin-like growth factor (IGF1) production. Local delivery of estrogen, on the other hand, would bypass first-pass metabolism and avoid alarming systemic side effects, making it an attractive alternative.

To develop targeted E2 delivery, we first synthesized E2–nanodiamond complexes (E2/ND) that were subsequently embedded in methacrylated glycol chitosan hydrogel (G). ND particles, which are capable of mediating improved efficacy and safety by forming complexes around the active agent while preserving its innate functionality (20–27). ND safety and biocompatibility have been clearly demonstrated in numerous applications ranging from oncology to wound healing (28–35). Similarly, hydrogels have been extensively used for tissue engineering and drug delivery applications due to their high biocompatibility (36). The application of G at the site of injection allows for the local delivery of bioactive molecules to tissue defects in a minimally invasive manner without the need for any surgical incisions (37–39). In addition, injectable G facilitates attachment of bioactive agents to the defect structure (40). Using this approach, we demonstrate E2/ND/G's ability to promote postexpansion palatine bone remodeling, leading to improved clinical success of palatal expansion. Our outcomes indicate that the E2/ND/G platform may represent a promising clinical tool for achieving superior postexpansion stability, addressing the pervasive complication in craniofacial medicine.

Results

ND/G Synthesis and Characterization. NDs were loaded with E2, using a conventional physisorption process that did not require modification to the drug or ND surface (Fig. 1*A*). Thermogravimetric analysis (TGA) was performed to confirm E2 loading on the NDs. A comparison of unmodified NDs and E2-loaded NDs revealed a clear difference in the TGA profile following drug loading (Fig. 1*B*). Based on the initial addition of 2 mg E2 and 5 mg ND, the comparison of mass ratios (26% of E2 to 68% of ND from analysis = 0.38; 0.4 for initial E2 to ND ratio), TGA revealed 95% binding of E2 to ND. Confirmation of sustained drug loading as well as release was assessed and visualized using E2/ND vials on a macroscopic scale at specific time points of 1 h, 2 h, 3 h, 4 h, 12 h, 48 h, 96 h, 120 h, 192 h, and 336 h. Drug and ND presence was visually confirmed at each time point, demonstrating the ability of the E2/ND/G to therapeutically address bone formation for a sustained period. The hydrogel properties such as gelation time, modulus, and cytotoxicity were confirmed as described in previous studies (41–43). Release of the E2 from NDs over time was quantified and confirmed using ELISA of the eluate (Fig. 1*C*). We found that in 1 h and 2 h, E2 was released abundantly with an amount of ≈400 μg. From 3 h to 336 h, the eluted E2 concentrations stabilized to ≈40 μg (Fig. 1*C*). The cumulative E2 release profile showed that 33% of loaded E2 was released over the first 24 h. These results along with the E2/ND/G imaging indicate that while a larger proportion of E2 was released at the initial stages of testing, prolonged release over multiple weeks was possible due to the sustained presence of loaded E2. These findings support the successful sustained delivery of E2 using the ND/G platform.

To examine the bioactivity of E2 released from ND, in vitro experiments using human mesenchymal stem cells isolated from bone marrow (BMSCs) were performed. BMSCs were induced to undergo osteogenic differentiation and a pro-osteogenic effect of E2 was compared by examining mRNA expression of osteogenic marker genes, *RUNX2*, *OCN*, and *DLX5*. Marked increases of osteogenic marker genes were found in both E2 and E2/ND groups compared with control and ND groups. There was no statistically significant difference observed between E2 and E2/ND groups, indicating the full bioactivity of E2 released from ND (Fig. 1*D*).

The toxicity and biological effects of dimethyl sulfoxide (DMSO) were also examined using BMSCs. BMSCs were treated with varying concentrations of DMSO (0.01%, 0.02%, 0.1%, 0.2%, and 1%) and

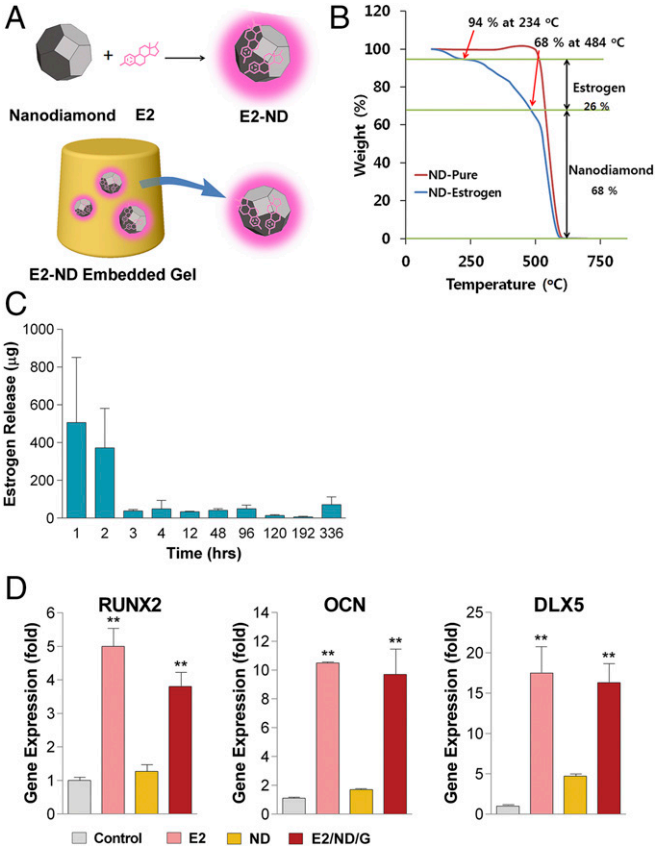

Fig. 1. (*A*) A schematic of E2/ND complex embedded within a hydrogel matrix. (*B*) Representative thermogravimetric analysis of pristine E2 (in red) vs. E2/ND complex (in blue). (*C*) Time-dependent E2 release from E2/ND/G using ELISA. (*D*) Expression of osteogenic marker genes, in vitro, used for validation of E2 functionality following release from NDs.

cell viabilities were measured by 3-(4,5-dimethylthiazol-2-yl)-2,5-diphenyltetrazolium bromide (MTT) assay at different time points (days 1, 2, 3, 4, 6, and 8). Compared with the control group, cell viability was compromised with 1% DMSO starting on day 3, but there was no statistical difference at lower concentrations (Fig. S1*A*). To investigate the potential effects of DMSO in osteogenic differentiation of BMSCs, BMSCs were induced to undergo osteogenic differentiation with DMSO treatment. One percent DMSO treatment significantly suppressed osteogenic differentiation and mineralization in BMSCs as shown in decreased alkaline phosphatase (ALP) staining and Alizarin Red staining (Fig. S1 *B* and *C*). There was no statistical difference in BMSC's osteogenic potential at lower concentrations.

Establishment of Midpalatal Suture Expansion and Relapse Model for Rats. Following preliminary experiments to determine the appropriate expander design for rats, we have successfully established an apparatus for palatal expansion and retention (Fig. 2 *A* and *B*). The expander was fabricated with a 0.014-inch stainless steel wire, consisting of a 1.5-mm helical spring and 7-mm extended arms. Extended arms were placed around the central incisors with a helical spring placed intraorally to reduce discomfort to the rats. The expander was cemented on 10 rats (6 wk old) to confirm its efficiency and stability. The rats underwent 7 d of 100-g force application and micro-CT images confirmed successful and sufficient separation of the midpalatal suture (Fig. 2 *C* and *D*). A total of 1.5–2 mm of clinical expansion was achieved without dislodgement of the appliance (Fig. 3 *A* and *B*). Micro-CT images demonstrated that the amount of skeletal separation of the midpalatal suture was

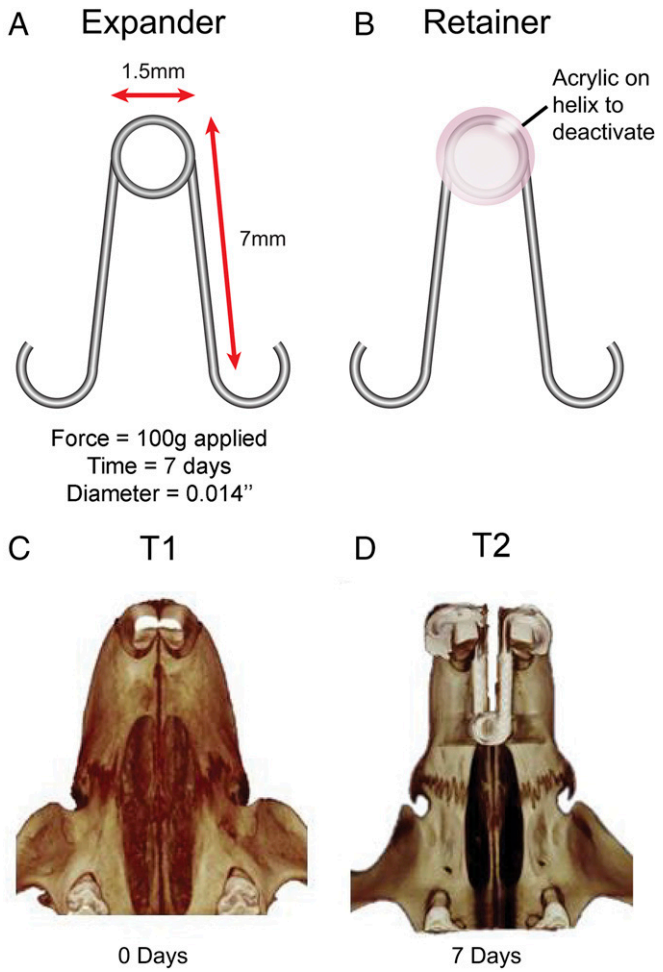

Fig. 2. (*A*) Visual representation of the intraoral self-activated expander with the active helix 1.5 mm in diameter and extension arms 7 mm in length bilaterally. The force of 100 g is exerted by compressing on the helical part of the spring for 7 d to achieve expansion. (*B*) Visual representation of the expander converted into the retention device at T2 by deactivating the helical spring with rigid acrylic resin. (*C*) Three-dimensional micro-CT image of the rat palate at T1. (*D*) Three-dimensional micro-CT image of the expanded rat palate at T2.

consistent with the amount of separation of the teeth. Furthermore, it was confirmed that the separation of the maxillary incisors was a result of the expansion of the palate with only negligible dental movements independent of skeletal expansion (Figs. 2*D* and 3*B*). This clinical and radiographical assessment of the expansion is particularly relevant in orthodontic clinical practice.

Direct measurements of the diastema, the distance between the gingival margins of maxillary incisors, revealed a very small SE at postexpansion (T2), suggesting a consistent expansion amount among all rats. Nevertheless, to further standardize the amount of expansion, we used the relapse ratio (amount of relapse per amount of expansion) in our analysis of stability of expansion. Furthermore, there was no significant difference in the amount of expansion at T2, compared with postretention (T3), indicating that the retention apparatus successfully retained initial expansion (Fig. 3*C*). At T3, the retention appliance was removed, allowing the sutural expansion to relapse freely, resulting in a significant decrease in diastema in all animals.

The animals showed no signs of discomfort, aberrant weight fluctuations, early mortality, or complications indicative of systemic E2 toxicity.

E2/ND/G Results in Significant Decrease in Clinical Relapse Following Midpalatal Expansion. The animals were divided into the control, E2 only, and E2/ND/G groups with each group further divided equally into retention and relapse groups (Fig. S2). The diastema of each rat's incisors was measured at four time points. Significant relapse was noted at T4 for all groups upon allowing the expanded maxillae to relapse freely. The relapse ratios for the control group and E2-only group were 40% and 30%, respectively. This amount of relapse is consistent with the clinical relapse seen in patients undergoing palatal expansion (9, 10). On the other hand, the E2/ND/G group exhibited just 13% relapse, a threefold decrease compared with the control group (Fig. 3*D*). There was no statistical difference in relapse ratio among the control group and the scaffold-only groups (ND/G and ND/G/DMSO) (Fig. S3*A*).

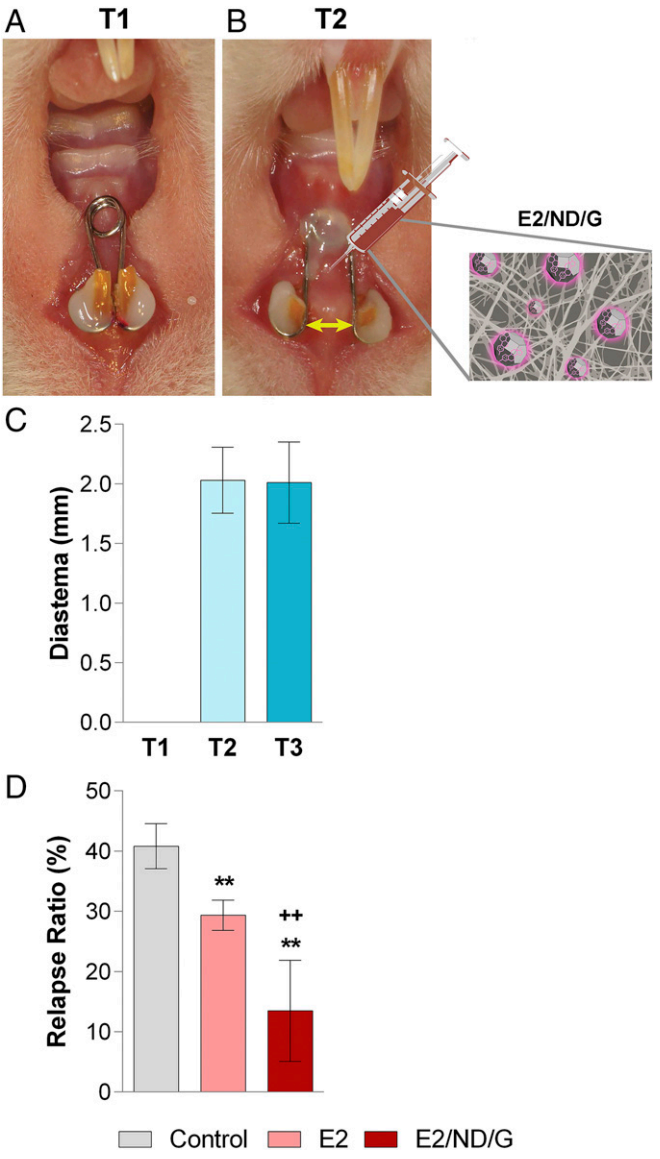

Fig. 3. (*A*) Intraoral view of expansion appliance cemented onto maxillary incisors at T1. Note no space between the incisors. (*B*) Intraoral view following 7 d expansion at T2. Diastema measurement is shown in yellow. Cartoon syringe demonstrates site of E2/ND/G injection. (*C*) Diastema measurement for the control group rats at T1, T2, and T3 time points. (*D*) Relapse ratio for the control, E2-only, and E2/ND/G groups. $^{**}P < 0.01$ between the control and E2 groups; $^{++}P < 0.01$ between the E2 and E2/ND/G groups.

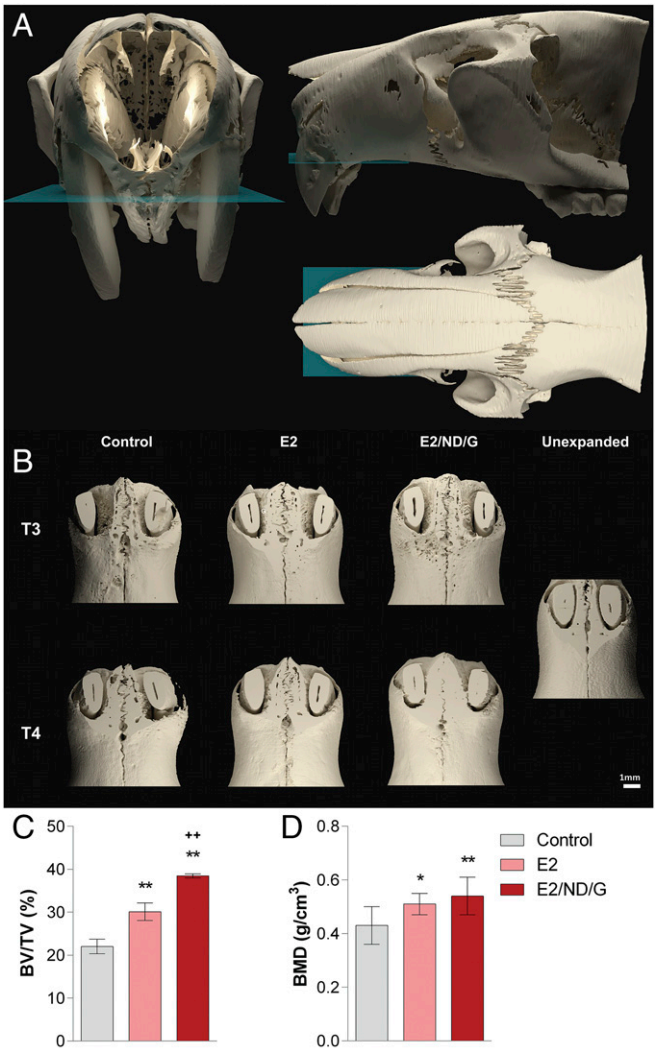

Fig. 4. (*A*) Three-dimensional volume rendering of a sample showing the level of slicing (green plane) in all dimensions. (*B*) Visual comparison at time points T3 (*Top* row) and T4 (*Bottom* row) for the control, E2-only, and E2/ND/G groups. (*C* and *D*) Volumetric analysis of BV/TV at T3 (*C*) and BMD at T4 (*D*) for all three groups. $^{*}P < 0.05$ and $^{**}P < 0.01$ between the control and E2 groups. $^{++}P < 0.01$ between the E2 and E2/ND/G groups.

E2/ND/G Facilitates Increase in Bone Mineral Density and Bone Volume. Micro-CT images were obtained to evaluate whether the decrease in postexpansion relapse was due to enhanced bone formation. Three-dimensional images were generated and volumetric analysis was performed to quantify bone volume and bone mineral density (BMD) (Fig. 4*A*). While micro-CT images of the control group revealed visually evident bone formation at the expanded region at T3, both E2-only and E2/ND/G groups displayed a more substantial increase in bone fill in the palate than the control group (Fig. 4*B*). In particular, a distinct visual comparison could be made between bone formation in the control and E2/ND/G groups at T4, as the E2/ND/G group demonstrated full restoration with bone in the expanded midpalatal suture while the E2-only and control groups displayed bone that remained porous (Fig. 4*B*).

Consistent with these findings, bone volume/tissue volume (BV/TV) was significantly greater in the E2/ND/G and E2-only groups compared with the control group after 14 d of retention. The E2/ND/G group had the greatest bone volume, a twofold increase from the control group and significantly higher than the E2-only group (Fig. 4*C*). Furthermore, an additional DMSO experiment showed no statistical difference in BV/TV among the control group and the scaffold only groups (ND/G and ND/G/DMSO), demonstrating that there were no biological effects of ND/G or DMSO exposure and DMSO utilization did not impact the functionality of E2/ND/G (Fig. S3*B*). Similarly, the E2-only and E2/ND/G groups demonstrated an increase in BMD compared with the control group at T4; however, there was no statistical difference between the two E2 groups (Fig. 4*D*).

E2/ND/G Is Associated with Increased Number of Osteoblastic Cells and Increased Bone Formation. To further validate our preclinical findings at the histological level, hematoxylin and eosin (H&E) staining was performed to verify E2/ND/G's osteogenic efficacy (Fig. 5 *A* and *B* and Fig. S2 *A* and *B*). Microscopic observation of the midpalatal suture in coronal sections revealed preosteoblastic mesenchymal cells within the suture with osteoid or woven bone forming around the margin of expanded borders in the palate. There were no remnants of ND or G particles detected in the midpalatal site at either T3 or T4.

The E2/ND/G group demonstrated advanced suture organization, interdigitation, and marked increase in bone fill compared with the control and E2-only groups (Fig. 5*A* and Fig. S4). The histological analysis also demonstrated an increase in the area of woven

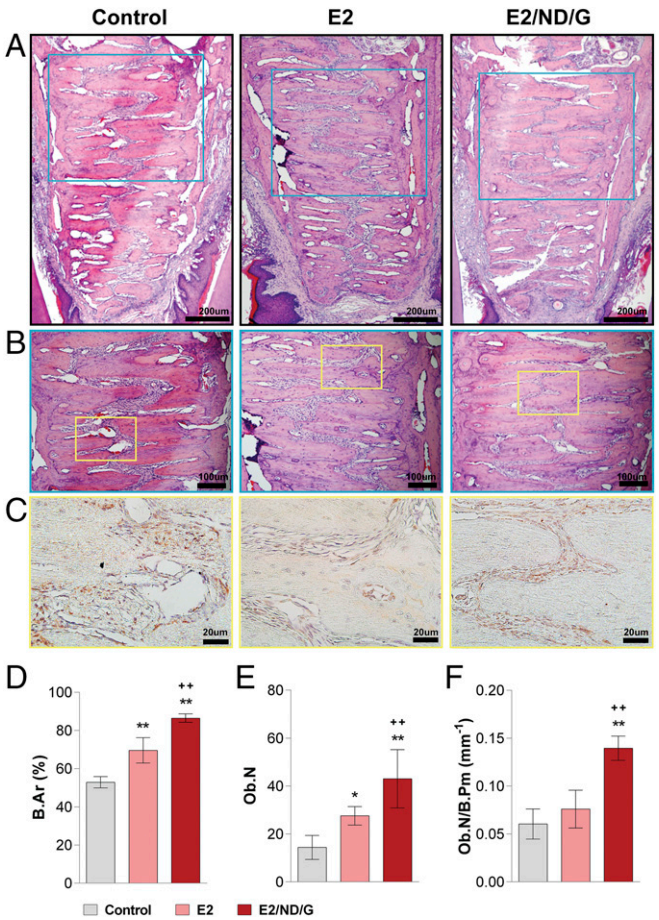

Fig. 5. Histological analysis at T4. (*A* and *B*) Representative H&E images for the control, E2, and E2/ND/G groups. Blue rectangle in *A* is the region that is magnified in *B*. Yellow rectangle in *B* is the region that is further magnified in *C*. (*C*) Representative osteocalcin IHC staining images for the control, E2, and E2/ND/G groups. (*D*) Quantification of B.Ar (mineralized area/total area × 100) for all three groups. (*E* and *F*) Quantification of osteoblast number (Ob.N) (*E*) and Ob.N per bone surface perimeter (B.Pm) (*F*). $^{*}P < 0.05$ and $^{**}P < 0.01$ between the control and E2 groups. $^{++}P < 0.01$ between the E2 and E2/ND/G groups.

bone arising from surrounding mesenchymal tissues and in the number of osteocytes for both the E2-only and E2/ND/G groups. Under higher magnification, the E2/ND/G group demonstrated a marked increase in neovascularization within the suture and normal bone structure, with osteocytes in lacunae and healthy marginal osteoblasts in the newly formed bony areas (Fig. 5*B*).

Similarly, histological quantification revealed that there was a significant increase in bone area (B.Ar) and osteoblast prevalence (Fig. 5 *D–F*). The number of osteoblasts lining the midpalatal suture [osteoblast number (Ob.N) per bone surface perimeter (B.Pm)] revealed a threefold increase in osteoblast number in the E2/ND/G group compared with the control group *(*Fig. 5 *E* and *F)*. In summary, histological evaluation confirmed enhanced osteogenic activity during postexpansion palatal bone remodeling with the application of E2/ND/G.

E2/ND/G Demonstrates Elevated Osteocalcin Expression Evidenced by Immunohistochemical Analysis. Additionally, immunohistochemical staining with osteocalcin (OCN) was performed to visualize osteoblastic activity and osteogenic progenitor cells during palatal expansion and relapse. A distinct comparison could be made among the groups (Fig. 5 *C* and *F*) in which the E2/ND/G group showed a dense compilation of positive preosteoblastic cells within the osteogenic zone in the suture as well as an increased number of OCN-positive cells lining the suture. The control group revealed sparse numbers of preosteoblast cells within the osteogenic zone as well as osteoblasts lining the suture. Notably, more OCN-positive cells with intensive staining were detected in the E2/ND/G group, reflecting the dynamic changes of local osteogenesis. These data provide an independent line of evidence that E2/ND/G has an osteogenic role, increasing the number of and stimulating the activity of osteoblasts.

E2/ND/G Platform Demonstrates Local Release of E2. While the localized enhancement of relapse prevention was clearly demonstrated preclinically, we performed an E2 systemic distribution experiment of the E2/ND/G platform to ensure its local delivery. An ovariectomized animal model was used to avoid E2-level fluctuations in females. Systemic release of E2 from E2/ND/G was quantified at three time points (2 h, 24 h, and 7 d) and confirmed using ELISA of the collected serum. A 2-h time point was selected as abundant E2 release from E2/ND/G was detected at this time (Fig. 1*C*). At 2 h, the E2/ND/G group demonstrated 20 pg/mL serum E2 concentration, which is a 150-fold decrease from the E2-only group (2,914 pg/mL) (Fig. 6). The serum E2 concentration for E2/ND/G was maintained in a stable range of 5–20 pg/mL while systemic E2 distribution from the E2-only group had a drastic decrease within 24 h.

Discussion

The problems suffered by patients with CLP are multifold, including nasal deformity, dental malocclusion, eating difficulty, speech disorders, and social alienation due to physical appearance. The complexity of treating this anomaly necessitates an interdisciplinary approach composed of multiple surgeries and outpatient care throughout a patient's life. As part of the craniofacial team that treats patients with CLP, orthodontists play an essential role in correcting the function and esthetics of the orofacial area. This encompasses the sequential treatment of maxillary expansion with bone graft surgery, which poses a major challenge due to postexpansion instability. Absence of bone in the cleft site makes new bone generation particularly difficult for these patients, resulting in high relapse rates, repeated surgeries, and prolonged orthodontic treatment. As enhancing bone formation in the midpalatal suture is known to be critical for preventing relapse, researchers have made numerous efforts to stimulate osteoblastic activity (44–49). However, no additional therapeutic modality is currently used in conjunction with palatal expanders due to the clinical infeasibility

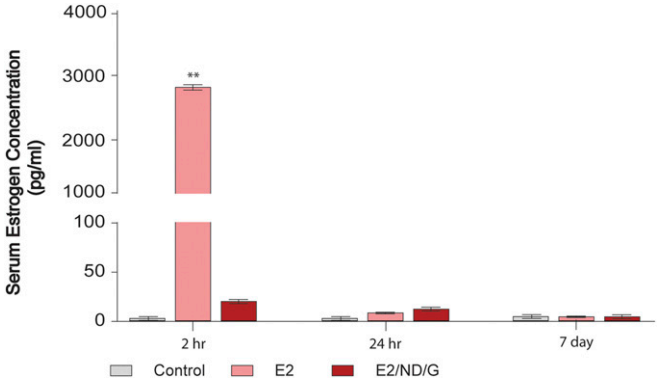

Fig. 6. Time-dependent serum E2 concentration using ELISA. $^{**}P < 0.01$ between the E2 and E2/NDG groups.

and safety concerns of previously proposed adjuvant agents. Therefore, we studied a well-established and economical anabolic agent, E2, delivered through a bioengineered nanotechnology platform.

To evaluate the role of the E2/ND/G complex in maxillary expansion and relapse, we first developed an animal model that could accurately represent clinical expansion. A previous study used a round bur to create holes in the incisors to secure an expander in place, causing unnecessary pain to the animals and compromising the design's stability from damages to the anchor teeth (49). Another design with an extraorally secured helix lacked reproducibility due to a high chance of failure as animals could easily tamper with the appliance (50). In contrast, our palatal expansion model involves placement of a self-activated spring around the incisors, rendering it more comfortable and secure for the animals. This design leverages the unique anatomy of the rat's long rooted incisors, which serve as stable anchors, facilitating efficient skeletal expansion. Our reproducible preclinical model (Fig. 2) circumvents shortcomings of previous designs and closely replicates skeletal palatal expansion in patients with CLP. Furthermore, our expansion analysis methods via measurements of the diastema and radiographic images using computed tomography closely mirror the clinical assessment methods used for patients with CLP undergoing expansion. Evidently, our design allows for the effective analysis of postexpansion stability and palatal bone remodeling, a potentially valuable model that can be used in future translational studies for craniofacial regeneration.

E2 is used for a wide array of therapeutic applications, including for treatment of dermatological diseases, osteoporosis, breast cancer, and prostatic carcinoma (51). Most E2 administration involves oral, transdermal, s.c., or i.v. injections, with the exception of the vaginal ring (52, 53). However, a local E2 delivery system specifically for skeletal effects has yet to be developed despite the fact that E2 has been well established as a key agent in bone health. E2 mediates its beneficial skeletal effects through multiple mechanisms, including its modulation of mesenchymal stromal cell differentiation into the osteoblast lineage (54) and promotion of osteoblast proliferation (55). However, clinical applications for E2's osteogenic effects are less appreciated due to pleiotropic effects from the ubiquitous presence of E2 receptors throughout the body. Thus, a local delivery of E2 is required to avoid the undesired effects of systemic E2 administration.

Finally, safety concerns of administering E2, especially to growing male patients, need to be addressed. It is important to note that endogenous E2 is critical in maintaining bone mineral density at all ages and in both genders (56–59). The undesired effects of E2 in males, such as suppression of testosterone, were observed only at high doses of 2 ~ 6 mg daily, while lower doses of E2 significantly promoted bone formation without such side effects (57). Low doses

of E2 (4–90 μg/d) in boys have been shown to stimulate ulnar growth (60) and play an essential role in bone development in both genders during the pubertal growth spurt (61–63). Due to the low dosing of E2 used in this study coupled with its local, slow release using the ND/G vehicle, our therapeutic approach may represent a clinical application with superior safety and efficacy.

In this work, we used ND technology and G to create a system for targeted and sustained delivery of E2. For its potential clinical use in the future, we have rigorously studied its properties to ensure its safety and feasibility. NDs were safely cleared through urinary and digestive excretion, depending on the mode of administration (23, 35, 64, 65). Importantly, ND vehicles complexed with gadolinium-based magnetic resonance imaging agents have resulted in being among the highest ever reported per-gadolinium relaxivity values (21). In addition, ND safety and biocompatibility have been recently demonstrated in a nonhuman primate study involving systemic administration of NDs to both genders, where no apparent toxicity or impaired organ function was observed (64). Similarly, the safety and biocompatibility of hydrogels allow for their versatile applications in tissue engineering (36–38, 66). Our photo–cross-linked chitosan hydrogel was degradable by lysozyme as confirmed in previous studies (41, 42). Furthermore, prior studies have shown that PEG-based hydrogels have tunable degradation rates and are well tolerated (66, 67), and the use of DMSO in our E2/ND/G platform was shown to have no biological effects or adverse toxicities. We used methacrylated glycol chitosan G, which enabled local delivery of E2/ND in a minimally invasive manner using blue-light assisted gelification. Such light curing avoids potential adverse effects associated with UV exposure that is required in polymerization of previous hydrogels (68) and it is routinely used in dental practice, adding to the applicability of this system.

Our findings clearly demonstrated that the E2/ND/G platform extended E2's pro-osteogenic effects with a single injection compared with every-other-day injections of unmodified E2, resulting in significantly superior postexpansion stability with reduced relapse and enhanced palatal bone remodeling (Figs. 4 and 5). E2/ND/G was able to deliver a consistent effective concentration of E2 at the injection site for prolonged therapeutic activity, thereby eliminating concerns regarding the systemic and pleiotropic effects of E2. The remarkable safety and biocompatibility of the E2/ND/G platform, coupled with its demonstrated osteogenic capacity, provide a powerful foundation for its continued development as an innovative clinical approach for care of patients with CLP.

Materials and Methods

E2/ND/G Synthesis. NDs that were ball milled and possessing a truncated octahedral architecture were obtained from the NanoCarbon Research Institute and initially characterized as previously described (23, 29). E2/ND was synthesized by a drying procedure (e.g., lyophilization) of homogeneously mixed E2 and ND. First, ND aqueous solution was dried, and the dried NDs were then redispersed in dimethyl-formamide (DMF) at a ratio of 5:1 (wt/vol). The DMF solution with NDs was sonicated for 40 min and then sterilized by autoclaving for about 1 h. A total of 5 mg of E2 in 1 mL of DMSO was subsequently added to the ND solution in DMF (ND: E2 = 1.5 mg: 0.6 mg). The solution was mixed homogeneously, lyophilized overnight, and then redispersed in 285 μL of DMSO. For E2/ND/G synthesis, methacrylated glycol chitosan (MGC) was prepared as described previously (69). The E2/ND was mixed homogenously with MGC in 1 mL water (ND: E2: polymer = 5 mg: 2.1 mg: 20 mg) followed by overnight lyophilization. The lyophilized sample was redispersed in 1.05 mL of a water and DMSO mixture with a ratio of 1:4 (vol/vol). To the solution, 50 μL of riboflavin (photo initiator) was added for the polymerization process of MGC. After these components were mixed homogeneously, it was polymerized using blue light for formation of E2/ND/G.

Release Profile of E2/ND. E2/ND/G containing 2 mg E2 was put in a vial followed by the addition of 2 mL 10% FBS solution diluted 1:1 with PBS. Then, the E2/ND/G in fresh media was incubated at 36.5 °C. E2 in the supernatant was collected at 1 h, 2 h, 3 h, 4 h, 12 h, 48 h, 96 h, 120 h, 192 h, and 336 h. After the collection of supernatant, the media of the E2/ND/G were replaced with fresh media followed by incubation. The collected samples were analyzed for E2 elution via ELISA (Estradiol ELISA Kit 582251; Cayman Chemicals), according to the manufacturer's protocols. Briefly, the samples and ELISA buffer were added into a precoated antibody 96-well plate and the plate was incubated for 1 h at room temperature. Wells were emptied and rinsed five times with washing buffer. Ellman's reagent was added and developed in the dark for 1 h. The plate's optical density (OD) value was recorded in a 415-nm wavelength.

Bioactivity of E2/ND. Human mesenchymal BMSCs were induced to undergo osteogenic differentiation, using osteogenic induction medium (OIM). OIM contained α-MEM (Invitrogen) supplemented with 10% FBS (Invitrogen), 50 μg/mL ascorbic acid, 5 mM β-glycerophosphate, and 100 nM dexamethasone (all from Sigma-Aldrich). OIM was changed every 2–3 d. For RUNX2 and DLX5, the cells were induced for 4 d and for OCN, the cells were induced for 7 d. The total RNA was isolated from cells using TRIzol reagents (Invitrogen). Two-microgram aliquots of RNAs were used to synthesize cDNAs, using random hexamers and reverse transcriptase according to the manufacturer's protocol (Invitrogen). The real-time PCR reactions were performed using the QuantiTect SYBR Green PCR kit (Qiagen) and the Icycler IQ Multicolor Real-time PCR Detection System (Bio-Rad). The primers for RUNX2 were forward, 5′-TGGTTACTGTCATGGCGGGTA-3; and reverse, 5′-TCTCAGATCGTTGAACCTTGCTA-3′. The primers for DLX5 were forward, 5′-GCTCTCAACCCCTACCAGTAT-3′; and reverse, 5′-CTTTGGTTTGCCATTCACCATTC-3′. The primers for OCN were forward, 5′-CAG ACACCATGAGGACCATC-3′; and reverse 5′-GGACTGAGCTCTGTGAG T-3′.

MTT Assay. Human mesenchymal stem cells were seeded in 96-well plates. After 24 h, cells were treated with different doses of DMSO (0.01%, 0.02%, 0.1%, 0.2%, and 1%) in culture medium. At different time points (days 1, 2, 3, 4, 6, and 8), 5 mg/mL MTT (Sigma-Aldrich) was added into the medium and incubated for 4 h at 37 °C. The MTT medium was discarded and cells were lysed in 100 μL of DMSO per well. The OD was measured at 570 nm, using a microplate reader.

ALP Staining and ALP Activity Assay. After osteogenic induction for 7 d, cells were fixed with 70% ethanol and incubated with a solution of 0.25% naphthol AS-BI phosphate and 0.75% Fast Blue BB (Sigma-Aldrich) dissolved in 0.1 M Tris buffer (pH 9.6). The ALP activity assay was performed using an ALP kit according to the manufacturer's protocol (Sigma-Aldrich) and normalized based on protein concentrations.

Alizarin Red Staining. After osteogenic induction for 2 wk, cells were fixed with 4% paraformaldehyde and stained with 2% Alizarin Red (Sigma-Aldrich). For quantification, Alizarin Red Stain (ARS) was destained with 10% cetylpyridinium chloride in 10 mM sodium phosphate for 30 min at room temperature. The optical absorbance was measured at 562 nm, using a microplate reader with a standard calcium curve in the same solution. The final calcium level in each group was normalized with the total protein concentrations prepared from a duplicate plate.

Animals. The animal protocol for this study was approved by the Animal Research Committee at the University of California, Los Angeles. A total of 42 female, 6-wk-old Sprague–Dawley rats with a mean weight of 180 ± 10 g were divided into three groups of 14 animals each: control group (n = 14), E2-only group (n = 14), and E2/ND/G group (n = 14). For the DMSO experiment, a total of 18 female, 6-wk-old Sprague–Dawley rats with a mean weight of 180 ± 10 g were divided into three groups: control group (n = 4), ND/G group (n = 7), and ND/G/DMSO group (n = 7). All three groups were further divided equally into retention group (T3) and relapse group (T4). For the E2 systemic distribution experiment, a total of 13 female, 6-wk-old ovariectomized Sprague–Dawley rats with a mean weight of 180 ± 10 g were divided into three groups: control group (n = 3), E2-only group (n = 5), and E2/ND/G group (n = 5). All animals were kept in a 12-h light and dark environment at a constant temperature of 23 °C and fed an ordinary, solid diet and water ad libitum. During 7 d of expansion, animals were given a soft diet. Body weight was measured every 7 d.

Expander Design and Expansion Procedure. A midpalatal expander was fabricated with 0.014-inch stainless steel wire with an intraoral helical spring 1.5 mm in diameter and 7-mm-long extended arms with loops that were secured to maxillary central incisors. Each expander was calibrated using a force gauge (Orthopli) to 100 g of force. Each rat was anesthetized with 4–5% Isothesia isoflurane gas (Henry Schein). TransbondPlus self-etching primer (3M Unitek) was applied to maxillary incisors. The expander was placed by wrapping the loops around each incisor, ensuring they were at the most gingival surfaces of maxillary central incisors. The expander was then secured onto the incisors, using light-cure flowable acrylic resin (Transbond Supreme LV Low Viscosity

Light Cure Adhesive; 3M Unitek). The expansion force was delivered to the midpalatal suture for 7 d without reactivation.

Preclinical Drug Delivery. After expansion, animals received a 0.05-mL local injection at the expanded midpalatal region with one of the following: vehicle, E2 solution, or E2/ND/G. The E2 group received every-other-day injections of 0.05 mL E2 solution for total of 90 μg E2 while the E2/ND/G group received a single injection of 0.05 mL E2/ND/G (90 μg E2) mixture, which was then cured with visible blue light (Valo Light Cure) for 15 s over the palatal tissue.

Retention and Relapse Procedure. Immediately following injections, the expanders were converted into retention devices for all rats by applying acrylic resin (Transbond Supreme LV Low Viscosity Light Cure Adhesive; 3M Unitek) onto the helical spring. All groups underwent 14 d of mechanical retention and the retention group was humanely killed after the retention period. The remaining rats from each group underwent relapse for 7 d after the entire appliances were removed. The relapse group animals were killed at the end of the relapse period.

Data collection.

Direct measurements. The distance between the maxillary incisors (diastema) at the gingival level was measured using a digital caliper (Orthopli) at four designated time points: (*i*) T1, preexpansion; (*ii*) T2, postexpansion; (*iii*) T3, retention; and (*iv*) T4, relapse. The relapse ratio was calculated according to the following formula (49):

$$\text{Relapse ratio} = (T4 - T3)/(T3 - T1) \times 100.$$

Micro-CT analysis. The maxilla was dissected and fixed with 4% (wt/vol) paraformaldehyde in 0.1 M PBS solution for 24 h. High-resolution micro-computed tomography (SkyScan 1172; SkyScan N.V.) was used to scan samples at a resolution of 15 μm, with a 70-kV and 141-μA X-ray source and a 0.5-mm aluminum filter. Three-dimensional image datasets were reconstructed from 2D X-ray images, using NRecon software (SkyScan N.V.) with image correction steps. Images of each sample were oriented on a 3D plane with DataViewer software (SkyScan N.V.). Three-dimensional volumetric analysis was conducted with CTAn software (SkyScan N.V.). To confirm consistency, a single individual repeated all analyses at two separate time points. The dataset was selected from the first appearance of palate to 120 sections down. The region of interest (ROI) was outlined with a trapezoid shape on consecutive transaxial sections to create a uniform volume of interest (VOI). BV/TV and BMD values were quantified.

Histological analysis. Samples were fixed in 4% paraformaldehyde (PFA) for 24 h and decalcified in 10% ethylenediaminetetraacetic acid (EDTA) (0.1 M, pH 7.1) solution at 4 °C for 3 wk. After decalcification, the palate was removed from the cranium using a scalpel and embedded in paraffin. Tissue samples were sectioned coronally in 5-μm sections and stained with H&E by the University of California, Los Angeles, Tissue Procurement Core Lab (TPCL). Sectioned immunohistochemistry (IHC) was carried out using anti-osteocalcin antibody (abcam; ab93876) as a primary antibody and 3-amino-9-ethylcarbazole (AEC) as a chromogen. An Olympus BX51 microscope and cellSens software version 1.6 (Olympus Corp.) were used to view and analyze results.

Serum E2 concentration. A total of 100 μL blood was collected from the tail vein of the animals at different time points (2 h, 24 h, and 7 d) and centrifuged at 9,391 × *g* for 1 min to separate serum. The collected samples were analyzed for E2 concentration via the mouse/rat estradiol ELISA kit (Calbiotech) according to the manufacturer's protocols. Briefly, the samples and ELISA buffer were added into a precoated antibody 96-well-plate and the plate was incubated for 2 h at room temperature. Wells were emptied and rinsed three times with washing buffer. TMB reagent was added and developed in the dark for 30 min. The plate's OD value was recorded in a 450-nm wavelength.

Statistical analysis. All data are presented as the mean ± SD for each group. Normal quantile plots were examined to confirm the data followed the normal Gaussian distribution, allowing the use of parametric methods. Therefore, means were compared using one-way analysis of variance (ANOVA) for statistical comparison among the three groups. The Fisher Least Significant Difference criterion under this model was used for the pairwise comparisons among the three groups. The α value was set to 0.05.

ACKNOWLEDGMENTS. We thank Dr. Kang Ting and his laboratory for generously providing the micro-CT machine and technical assistance and Dr. Jeff Gornbein for performing statistical analysis. We also thank Tania Ohebsion, Jaime Tran, Alex Lee, Tim Yu, Steven Kim, Michelle Wong, Armin Miresmaili, and Delano Hankins for their assistance during the surgeries. C.H. gratefully acknowledges support from the American Association of Orthodontists Foundation Biomedical Research Award and the National Institutes of Health/National Institute of Dental and Craniofacial Research (NIH/NIDCR) K08 Award (K08DE024603). D.H. gratefully acknowledges support from the National Science Foundation CAREER Award (CMMI-1350197), the Center for Scalable and Integrated NanoManufacturing (DMI-0327077), CMMI-0856492, DMR-1343991, OISE-1444100, the V Foundation for Cancer Research Scholars Award, the Wallace H. Coulter Foundation Translational Research Award, National Cancer Institute Grant U54CA151880 (the content is solely the responsibility of the authors and does not necessarily represent the official views of the National Cancer Institute or the National Institutes of Health), the Society for Laboratory Automation and Screening Endowed Fellowship, Beckman Coulter Life Sciences, and the American Academy of Implant Dentistry Research Foundation under Grant 20150460.

1. Stoll C, Alembik Y, Dott B, Roth MP (2000) Associated malformations in cases with oral clefts. *Cleft Palate Craniofac J* 37:41–47.
2. Arosarena OA (2007) Cleft lip and palate. *Otolaryngol Clin North Am* 40:27–60, vi.
3. Bergland O, Semb G, Abyholm FE (1986) Elimination of the residual alveolar cleft by secondary bone grafting and subsequent orthodontic treatment. *Cleft Palate J* 23:175–205.
4. Slaughter WB, Pruzansky S (1954) The rationale for velar closure as a primary procedure in the repair of cleft palate defects. *Plast Reconstr Surg* 13:341–357.
5. Long RE, Semb G, Shaw WC (2000) Orthodontic treatment of the patient with complete clefts of lip, alveolus, and palate: Lessons of the past 60 years. *Cleft Palate Craniofac J* 37:533.
6. Subtelny JD, Brodie AG (1954) An analysis of orthodontic expansion in unilateral cleft lip and cleft palate patients. *Am J Orthod Dentofac* 40:686–697.
7. Moussa R, O'Reilly MT, Close JM (1995) Long-term stability of rapid palatal expander treatment and edgewise mechanotherapy. *Am J Orthod Dentofacial Orthop* 108:478–488.
8. Mew J (1983) Relapse following maxillary expansion. A study of twenty-five consecutive cases. *Am J Orthod* 83:56–61.
9. Linder-Aronson S, Lindgren J (1979) The skeletal and dental effects of rapid maxillary expansion. *Br J Orthod* 6:25–29.
10. Stockfisch H (1969) Rapid expansion of the maxilla–success and relapse. *Rep Congr Eur Orthod Soc* 1969:469–481.
11. Ramstad T, Jendal T (1997) A long-term study of transverse stability of maxillary teeth in patients with unilateral complete cleft lip and palate. *J Oral Rehabil* 24:658–665.
12. Nicholson PT, Plint DA (1989) A long-term study of rapid maxillary expansion and bone grafting in cleft lip and palate patients. *Eur J Orthod* 11:186–192.
13. Prestwood KM, Kenny AM, Unson C, Kulldorff M (2000) The effect of low dose micronized 17ss-estradiol on bone turnover, sex hormone levels, and side effects in older women: A randomized, double blind, placebo-controlled study. *J Clin Endocrinol Metab* 85:4462–4469.
14. Prestwood KM, Kenny AM, Kleppinger A, Kulldorff M (2003) Ultralow-dose micronized 17beta-estradiol and bone density and bone metabolism in older women: A randomized controlled trial. *JAMA* 290:1042–1048.
15. Santen RJ, et al.; Endocrine Society (2010) Postmenopausal hormone therapy: An Endocrine Society scientific statement. *J Clin Endocrinol Metab* 95:s1–s66.
16. Weissberger AJ, Ho KK, Lazarus L (1991) Contrasting effects of oral and transdermal routes of estrogen replacement therapy on 24-hour growth hormone (GH) secretion, insulin-like growth factor I, and GH-binding protein in postmenopausal women. *J Clin Endocrinol Metab* 72:374–381.
17. Ruggiero RJ, Likis FE (2002) Estrogen: Physiology, pharmacology, and formulations for replacement therapy. *J Midwifery Womens Health* 47:130–138.
18. Gomes MP, Deitcher SR (2004) Risk of venous thromboembolic disease associated with hormonal contraceptives and hormone replacement therapy: A clinical review. *Arch Intern Med* 164:1965–1976.
19. Scarabin PY, Oger E, Plu-Bureau G; EStrogen and THromboEmbolism Risk Study Group (2003) Differential association of oral and transdermal oestrogen-replacement therapy with venous thromboembolism risk. *Lancet* 362:428–432.
20. Man HB, Lam R, Chen M, Osawa E, Ho D (2012) Nanodiamond-therapeutic complexes embedded within poly(ethylene glycol) diacrylate hydrogels mediating sequential drug elution. *Phys Status Solidi A Appl Mater Sci* 209:1811–1818.
21. Chow EK, Ho D (2013) Cancer nanomedicine: From drug delivery to imaging. *Sci Transl Med* 5:216rv4.
22. Wang X, et al. (2014) Epirubicin-adsorbed nanodiamonds kill chemoresistant hepatic cancer stem cells. *ACS Nano* 8:12151–12166.
23. Chow EK, et al. (2011) Nanodiamond therapeutic delivery agents mediate enhanced chemoresistant tumor treatment. *Sci Transl Med* 3:73ra21.
24. Ho D, Wang CH, Chow EK (2015) Nanodiamonds: The intersection of nanotechnology, drug development, and personalized medicine. *Sci Adv* 1:e1500439.
25. Smith AH, et al. (2011) Triggered release of therapeutic antibodies from nanodiamond complexes. *Nanoscale* 3:2844–2848.
26. Huang H, Pierstorff E, Osawa E, Ho D (2007) Active nanodiamond hydrogels for chemotherapeutic delivery. *Nano Lett* 7:3305–3314.
27. Xi G, et al. (2014) Convection-enhanced delivery of nanodiamond drug delivery platforms for intracranial tumor treatment. *Nanomedicine* 10:381–391.
28. Mochalin VN, Shenderova O, Ho D, Gogotsi Y (2011) The properties and applications of nanodiamonds. *Nat Nanotechnol* 7:11–23.
29. Barnard AS (2008) Self-assembly in nanodiamond agglutinates. *J Mater Chem* 18: 4038–4041.
30. Barnard AS (2009) Diamond standard in diagnostics: Nanodiamond biolabels make their mark. *Analyst* 134:1751–1764.

31. Adnan A, et al. (2011) Atomistic simulation and measurement of pH dependent cancer therapeutic interactions with nanodiamond carrier. *Mol Pharm* 8:368–374.
32. Kruger A (2005) Unusually tight aggregation in detonation nanodiamond: Identification and disintegration. *Carbon* 43:1722–1730.
33. Zhang Q, et al. (2011) Fluorescent PLLA-nanodiamond composites for bone tissue engineering. *Biomaterials* 32:87–94.
34. Mochalin VN, et al. (2013) Adsorption of drugs on nanodiamond: Toward development of a drug delivery platform. *Mol Pharm* 10:3728–3735.
35. Mohan N, Chen CS, Hsieh HH, Wu YC, Chang HC (2010) In vivo imaging and toxicity assessments of fluorescent nanodiamonds in Caenorhabditis elegans. *Nano Lett* 10: 3692–3699.
36. Hoare TR, Kohane DS (2008) Hydrogels in drug delivery: Progress and challenges. *Polymer* 49:1993–2007.
37. Hu J, et al. (2012) Visible light crosslinkable chitosan hydrogels for tissue engineering. *Acta Biomater* 8:1730–1738.
38. Drury JL, Mooney DJ (2003) Hydrogels for tissue engineering: Scaffold design variables and applications. *Biomaterials* 24:4337–4351.
39. Brandl F, Sommer F, Goepferich A (2007) Rational design of hydrogels for tissue engineering: Impact of physical factors on cell behavior. *Biomaterials* 28:134–146.
40. Watson BM, et al. (2015) Biodegradable, phosphate-containing, dual-gelling macromers for cellular delivery in bone tissue engineering. *Biomaterials* 67:286–296.
41. Park H, Choi B, Hu J, Lee M (2013) Injectable chitosan hyaluronic acid hydrogels for cartilage tissue engineering. *Acta Biomater* 9:4779–4786.
42. Choi B, Kim S, Lin B, Wu BM, Lee M (2014) Cartilaginous extracellular matrix-modified chitosan hydrogels for cartilage tissue engineering. *ACS Appl Mater Interfaces* 6: 20110–20121.
43. Choi B, et al. (2015) Visible-light-initiated hydrogels preserving cartilage extracellular signaling for inducing chondrogenesis of mesenchymal stem cells. *Acta Biomater* 12:30–41.
44. Amini F, Najaf Abadi MP, Mollaei M (2015) Evaluating the effect of laser irradiation on bone regeneration in midpalatal suture concurrent to rapid palatal expansion in rats. *J Orthod Sci* 4:65–71.
45. DeCesare GE, et al. (2011) Novel animal model of calvarial defect in an infected unfavorable wound: Reconstruction with rhBMP-2. *Plast Reconstr Surg* 127:588–594.
46. Uysal T, Amasyali M, Enhos S, Sonmez MF, Sagdic D (2009) Effect of ED-71, a new active vitamin D analog, on bone formation in an orthopedically expanded suture in rats. A histomorphometric study. *Eur J Dent* 3:165–172.
47. Cowan CM, et al. (2006) Nell-1 induced bone formation within the distracted intermaxillary suture. *Bone* 38:48–58.
48. Ekizer A, Yalvac ME, Uysal T, Sonmez MF, Sahin F (2015) Bone marrow mesenchymal stem cells enhance bone formation in orthodontically expanded maxillae in rats. *Angle Orthod* 85:394–399.
49. Sawada M, Shimizu N (1996) Stimulation of bone formation in the expanding mid-palatal suture by transforming growth factor-beta 1 in the rat. *Eur J Orthod* 18:169–179.
50. Zahrowski JJ, Turley PK (1992) Force magnitude effects upon osteoprogenitor cells during premaxillary expansion in rats. *Angle Orthod* 62:197–202.
51. Harrison RF, Bonnar J (1980) Clinical uses of estrogens. *Pharmacol Ther* 11:451–467.
52. Lindahl SH (2014) Reviewing the options for local estrogen treatment of vaginal atrophy. *Int J Womens Health* 6:307–312.
53. Weisberg E, et al. (2005) Endometrial and vaginal effects of low-dose estradiol delivered by vaginal ring or vaginal tablet. *Climacteric* 8:83–92.
54. Ernst M, Schmid C, Froesch ER (1988) Enhanced osteoblast proliferation and collagen gene expression by estradiol. *Proc Natl Acad Sci USA* 85:2307–2310.
55. Okazaki R, et al. (2002) Estrogen promotes early osteoblast differentiation and inhibits adipocyte differentiation in mouse bone marrow stromal cell lines that express estrogen receptor (ER) alpha or beta. *Endocrinology* 143:2349–2356.
56. Turner RT, Riggs BL, Spelsberg TC (1994) Skeletal effects of estrogen. *Endocr Rev* 15: 275–300.
57. Mueller A, et al. (2005) High dose estrogen treatment increases bone mineral density in male-to-female transsexuals receiving gonadotropin-releasing hormone agonist in the absence of testosterone. *Eur J Endocrinol* 153:107–113.
58. Steiniche T, et al. (1989) A randomized study on the effects of estrogen/gestagen or high dose oral calcium on trabecular bone remodeling in postmenopausal osteoporosis. *Bone* 10:313–320.
59. Cauley JA, et al.; Study of Osteoporotic Fractures Research Group (1995) Estrogen replacement therapy and fractures in older women. *Ann Intern Med* 122:9–16.
60. Caruso-Nicoletti M, et al. (1985) Short term, low dose estradiol accelerates ulnar growth in boys. *J Clin Endocrinol Metab* 61:896–898.
61. Ohlsson C, Vandenput L (2009) The role of estrogens for male bone health. *Eur J Endocrinol* 160:883–889.
62. Rochira V, Kara E, Carani C (2015) The endocrine role of estrogens on human male skeleton. *Int J Endocrinol* 2015:165215.
63. Rochira V, Balestrieri A, Faustini-Fustini M, Carani C (2001) Role of estrogen on bone in the human male: Insights from the natural models of congenital estrogen deficiency. *Mol Cell Endocrinol* 178:215–220.
64. Moore L, et al. (2016) Biocompatibility assessment of detonation nanodiamond in non-human primates and rats using histological, hematologic, and urine analysis. *ACS Nano* 10:7385–7400.
65. Liu Z, Tabakman S, Welsher K, Dai H (2009) Carbon nanotubes in biology and medicine: In vitro and in vivo detection, imaging and drug delivery. *Nano Res* 2:85–120.
66. Wassenaar JW, et al. (2016) Evidence for mechanisms underlying the functional benefits of a myocardial matrix hydrogel for post-MI treatment. *J Am Coll Cardiol* 67:1074–1086.
67. Grover GN, et al. (2015) Binding of anticell adhesive oxime-crosslinked PEG hydrogels to cardiac tissues. *Adv Healthc Mater* 4:1327–1331.
68. Xavier JR, et al. (2015) Bioactive nanoengineered hydrogels for bone tissue engineering: A growth-factor-free approach. *ACS Nano* 9:3109–3118.
69. Kim S, et al. (2016) Photocrosslinkable chitosan hydrogels functionalized with the RGD peptide and phosphoserine to enhance osteogenesis. *J Mater Chem B Mater Biol Med* 4:5289–5298.